coatings

MDPI

Article

λ/4–λ/4 Double-Layer Broadband Antireflective Coatings with Constant High Transmittance

Hanxi Liu [1], Pingmei Wang [2,3], Qianyang Fan [1], Jianhui Luo [2,3], Peiwen Xiao [2,3] and Bo Jiang [1,*]

[1] Key Laboratory of Green Chemistry & Technology of Ministry of Education, College of Chemistry, Sichuan University, Chengdu 610064, China; 2019222030138@stu.scu.edu.cn (H.L.); fanqianyang@stu.scu.edu.cn (Q.F.)
[2] Research Institute of Petroleum Exploration & Development (RIPED), CNPC, Beijing 100083, China; wangpm@petrochina.com.cn (P.W.); luojh@petrochina.com.cn (J.L.); xiaopw@petrochina.com.cn (P.X.)
[3] Key Laboratory of Nano Chemistry (KLNC), CNPC, Beijing 100083, China
* Correspondence: jiangbo@scu.edu.cn

Abstract: Antireflective (AR) coatings can suppress the undesired interfacial Fresnel reflections, and they are widely used in optical devices and energy-related instruments. Conventional single-layer AR coatings, which only work at a single wavelength, encounter serious limitations in some practical applications because of their inherent properties. In this paper, λ/4–λ/4 double-layer antireflective (AR) coatings with constant high transmittance in a pre-determined wavelength range was prepared by the sol–gel method via acid-catalyzed and base-catalyzed SiO_2 thin films. A double-layer antireflective coating with an almost constant transmittance value of 99.8% in the range of 550–700 nm was obtained, and the transmittance of this coating was higher than 99% in a wider range of 450–850 nm with a fluctuation of less than 1%. The coatings had good environmental stability and maintained constant high transmittance after two weeks of exposure in 50% humidity. The broadband AR coatings may have important applications in fields such as electroluminescent display.

Keywords: broadband antireflective coatings; silicon dioxide; thin film design

Citation: Liu, H.; Wang, P.; Fan, Q.; Luo, J.; Xiao, P.; Jiang, B. λ/4–λ/4 Double-Layer Broadband Antireflective Coatings with Constant High Transmittance. *Coatings* **2022**, *12*, 435. https://doi.org/10.3390/coatings12040435

Academic Editor: Valentin Craciun

Received: 11 February 2022
Accepted: 21 March 2022
Published: 24 March 2022

1. Introduction

Antireflection coatings (ARCs) can significantly reduce optical loss by making use of phase changes and dependence of the reflectivity on the refraction index, and are widely used in various applications such as display panels, camera lenses, architectural glass, solar cells, and high-power laser systems [1–8]. The light reflection of a single side of the glass–air interface is about 4–5%, and for both sides of the glass–air interface, the light reflection approaches 8–10%. ARCs applied to display panels demand constant high transmittance with little fluctuation because display panels are sensitive to chromatic aberration. A single-layer ARC can be non-reflective only at a specific wavelength, which means it is severely limited in a slice of a special optical device.

Driven by the demand for ARCs with better antireflective characteristics, multilayer ARCs have become a research hotspot. Zhang et al. reported a λ/4–λ/4 double-layer ARC with an excellent optical performance, of which the transmittance can attain 99.95% at 532 nm and almost 100.00% at 1064 nm [9]. Li et al. prepared a λ/4–λ/2 double-layer broadband ARC with an average transmittance of 99.4% at 500–700 nm using the sol–gel method [10]. Li et al. also prepared a λ/4–λ/2–λ/4 triple-layer ARC which can attain consistently high transmittances, and the average transmittance was 99.4% at 500–700 nm [11].

The practical problem is that it is hard to prepare a double-layer ARC that can attain consistently high transmittances in a predetermined wavelength range with little transmittance fluctuation. Transmission spectra of most double-layer ARCs have two or more peaks, which means they can attain high transmittance only at some specific wavelengths. An optical coating devoted to the reduction in display panel specular reflection should be

developed with consistently high transmittances and a simple process. There are a variety of techniques for making thin coatings. Sputtering can be used to deposit thin layers on many kinds of substrates with different shapes [12,13]. It is a well-developed process for the deposition of ARCs on thermochromic windows and display devices [14–17]. However, sputtering requires a moderate vacuum for deposition. Physical vapor deposition and chemical vapor deposition are typically used to form layers with controlled thicknesses and refractive indexes [18,19]. It remains challenging to extend this technology for broader applications because of the relatively high cost and substrate size limitations of the vapor deposition technique. Compared with these methods, the sol–gel method has the advantages of controllable microstructure, low cost, simple operation process, and the application of substrates with different sizes and shapes. With a controllable microstructure, specific properties such as ultra-low refractive index and hydrophobic performance can be easily achieved.

In this work, the λ/4–λ/4 double-layer ARCs with excellent optical properties were fabricated by a simple sol–gel dip-coating process. The refractive index and thickness of the double-layer coatings were designed with computer film design software (TFCalc™, version 3.5). Substrates (BK-7 glass) coated with the double-layer ARC attained constant high transmittance of 99.8% with a fluctuation of 0.1% in the region of 550–700 nm and average transmittance of 99.25% in a wider region of 450–850 nm for the first time. This double-layer ARC remained almost intact after being placed for two weeks at 25 °C and 50% relative humidity. Thus, the double-layer ARC with multifunctional properties of constant high transmittance, broadband antireflection, and good environmental stability was successfully realized and it can have potential value, especially in the field of display panels.

2. Experimental Section

2.1. Preparation of Acid-Catalyzed Silica Sol

Tetraethyl silicate (TEOS) (97%, TCI, Japan), Methyltriethoxysilane (MTES) (98%, TCI, Japan), EtOH (double distillation, Changzhen, China), hydrochloric acid (HCl) (36%, Kelong, China) and H_2O (deionized water, Ulupure, China) were added into a clean PET container. The mixture was stirred for 2 h and the temperature was kept at 30 °C. Themolar ratio of (TEOS + MTES):EtOH:HCl:H_2O was 1:37.54:0.00408:4, and the proportion of MTES is in the range of 0–40%. After stirring for 2 h, the sols were stored in a thermostat for 7 days at 25 °C.

2.2. Preparation of Base-Catalyzed Silica Sol

Tetraethyl silicate (TEOS) (97%, TCI, Japan), Methyltriethoxysilane (MTES) (98%, TCI, Japan), EtOH (double distillation, Changzhen, China), $NH_3 \cdot H_2O$ (25%, Kelong, China) and H_2O (deionized water, Ulupure, China) were added into a clean PET container. The mixture was stirred for 2 h and the temperature was kept at 30 °C. The final molar ratio of TEOS:MTES:EtOH:$NH_3 \cdot H_2O$:H_2O was 0.91:0.09:37.6:0.17:3.25. After stirring for 2 h, the sols were stored in a thermostat for seven days at 25 °C. In order to remove the ammonia and prevent gelation or precipitation of sols, the silica sols were under refluxing in oil bath at 110 °C for 2 days. After removing ammonia, the sol was diluted to twice the mass.

2.3. Preparation of Films

The circular BK-7 glass with a diameter of 35 mm and a thickness of 3 mm were used as substrates, and the refractive index of BK-7 was 1.52. The substrates were immersed in EtOH for 30 s and we wiped with cleanroom wipers (LTK, Wuxi, China) carefully before the dip-coating process. The sols were deposited on the BK-7 under the condition of 30% relative humidity and 25 °C by the dip-coating method. The thickness of each layer can be controlled by regulating withdrawal rates in the dip-coating process. The bottom layer was deposited on the surface of bare substrates by dip-coating at a rate of 4200 μm/s and then heated at 400 °C for 2 h. The top layer was deposited on the bottom layer at a rate of 3600 μm/s.

2.4. Characterization of Double-Layer Coatings

The refractive indexes (n) of these coatings were measured on the ellipsometry (Horiba, Uvisel, error $\leq$ 2%) at λ = 500 nm. Transmission spectra were measured by a UV–Vis spectrophotometer (Lambda750, PerkinElmer, Waltham, MA, USA), and transmittance error $\leq$ 0.2%, wavelength $\leq$ 0.1 nm was used to measure the transmission spectra. Surface morphologies and cross-sections of the ARCs were investigated by scanning electron microscope (SEM) (Nova NanoSEM450, FEI, Hillsboro, OR, USA), which was used to investigate the surface morphologies and cross-sections of the ARCs. The surface roughness of the ARCs was investigated by atomic force microscopy (AFM) (Bruker Dimension Icon, Bruker, Billerica, MA, USA) and was used to investigate the surface roughness of the ARCs.

3. Results and Discussion

3.1. Design of Broadband ARCs with Constant High Transmittance

In various double-layer broadband ARC systems, $\lambda/4$–$\lambda/4\lambda/2$ (the central wavelength) and $\lambda/4$–$\lambda/2\lambda/4$ coating designs are the most commonly adopted in general. The λ refer to the desired central wavelength of ARCs. The $\lambda/4$–$\lambda/4$ coatings refer to two optical coatings with different refractive indexes and the thickness of each coating is $\lambda/4$. Compared with $\lambda/4$–$\lambda/2$ coatings, the $\lambda/4$–$\lambda/4$ coatings are better to achieve broadband ARCs with constant high transmittance [20].

$\lambda/4$–$\lambda/4$ double-layer broadband ARC with constant high transmittance is simulated by the computer software TFCalc™ (Version 3.5, Software Spectra, Spectra, Portland, OR, USA). For the double-layer ARCs, the desired central wavelength of each layer is 600 nm. Double-layer coatings with different refractive indexes are simulated and the results are shown in Figure 1. The optimum refractive index of the bottom layer and top layer are 1.40 and 1.145. The optimum simulated double-layer coating can achieve a constant high transmittance of 99.99% at a broadband wavelength of 550–700 nm and an average transmittance of 99.75% at a broader wavelength range of 450–850 nm. The thickness of the bottom and top layers are 107 nm and 131 nm, respectively, in the ideal model.

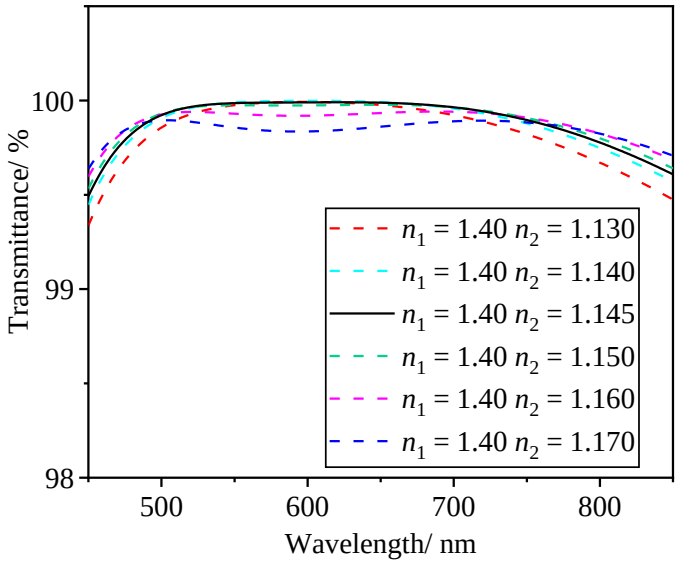

Figure 1. Simulated transmittance spectra of modeled double-layer coatings.

The preparation of sol–gel films can be achieved by various methods. The dip-coating method was adopted in our work because of the advantages of simple process, mild coating conditions, easy control of film thickness, and suitability for large-scale production, so it is widely used [21]. As shown in Scheme 1, the bottom layer was acid-catalyzed SiO_2 thin films and prepared by the dip-coating method and heating for 2 h at 400 °C (process I). The top layer was base-catalyzed SiO_2 thin films and prepared by the dip-coating method (process II).

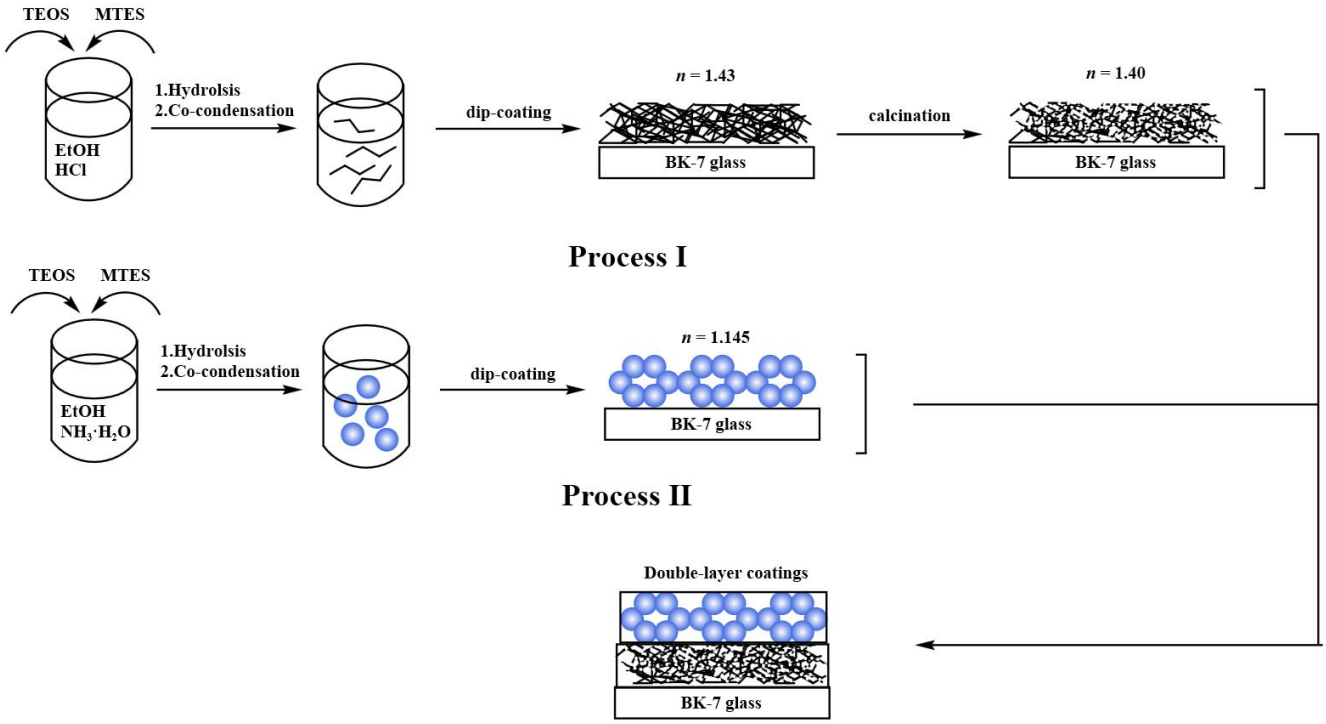

Scheme 1. Schematic illustration of bottom layer (process I), top layer (process II), and double-layer coatings.

3.2. Preparation of Bottom Layer and Top Layer

Several acid-catalyzed sols were prepared with different ratios of TEOS and MTES and the total amount of precursors remains unchanged. The ratios of TEOS:MTES are 9:1, 8:2, 7:3, and 6:4, respectively. The refractive indices of these coatings are shown in Figure 2.

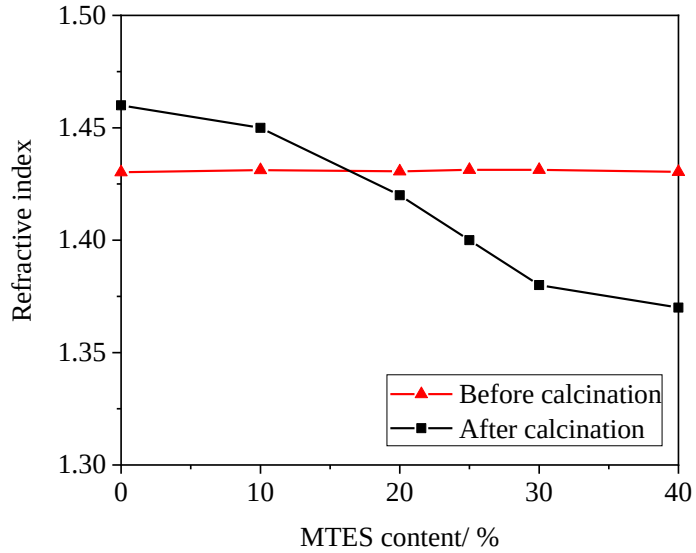

Figure 2. Refractive index changes before and after calcination of MTES with different content.

By comparing the refractive indexes of different ratios of MTES/TEOS sols, we found that the ratio of TEOS and MTES has no effect on the refractive indexes of these films before calcination with a refractive index value of 1.43. The refractive index of the film is determined by the size and shape of particles in the sol. It is reported that the particles of acid-catalyzed sol particles are generally chain-like, formed by incomplete hydrolysis of precursors [9,22]. According to the Reaction Limited Cluster–cluster Aggregation (RLCA)

model [23], the growth of the sol particles results in a linear chains structure. The size of sol particles is very small with particle–particle bonding, and thus the film formed by sol particles tends to be dense and robust. The synthesis of SiO_2 linear chains structure by the sol–gel process involves hydrolysis reactions and condensation reactions, which refer to the hydrolysis of precursors and the formation of Si–O–Si bonds. Compared with TEOS, there are only three ethoxy groups that can hydrolyze during the reaction in MTES instead of four. As only two ethoxy groups are needed during incomplete hydrolysis of precursors, TEOS and MTES may be regarded as the same, their ratios should theoretically have no influence on the refractive indexes of the film.

In Figure 2, refractive indexes obtained by spectroscopic ellipsometry analyses are reported for the various molar ratios of TEOS and MTES. As the MTES content increases from 0 to 40%, the refractive indexes of calcined films decrease gradually. There are two processes during calcination [24–26]. The porosity of calcined films increases and the refractive indexes of calcined films decrease because of decomposition reaction with the methyl group of MTES. On the contrary, the porosity of calcined films decreases, and the refractive indexes of calcined films increase because of condensation reaction with the hydroxyl group of TEOS. As the total number of precursors remains unchanged, more MTES means more methyl groups and fewer hydroxyl groups, and the apparent refractive indexes of the calcined films decrease as the MTES content increases.

Figure 3 displays the surface SEM images of 25% MTES film before and after calcination. The SEM images show that the porosity of the 25% MTES film becomes higher after calcination, which can explain the decrease in the refractive index of the film from 1.43 to 1.40. Therefore, we chose the film with 25% MTES content as the bottom layer for the double-layer ARC.

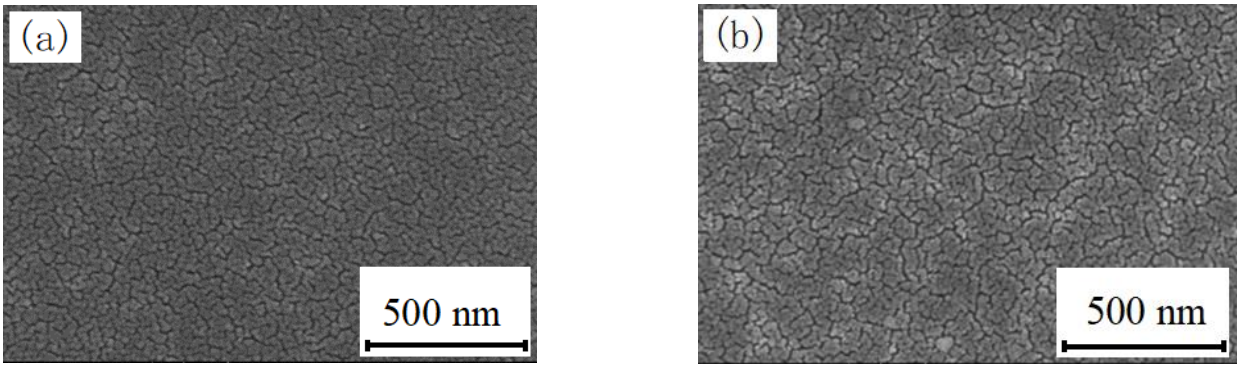

Figure 3. SEM images of 25% MTES film before calcination (**a**) and SEM images of 25% MTES film after calcination (**b**).

For the top layer of the double-layer ARC, an optical material with a refractive index of 1.145 is required. Our laboratory previously reported a silicate film with an adjustable refractive index from 1.21 to 1.10 via the sol–gel method [26]. MTES was introduced into the base-catalyzed film to decrease the refractive index of pure TEOS sol-based film. When MTES/TEOS = 0.1, the refractive index of the base-catalyzed film is exactly 1.145. This procedure was adopted in our work to prepare the top layer.

3.3. Optical Performance of the Double-Layer ARC

In the sol–gel dip-coating process, the film thickness can be easily controlled by withdrawal rate [21], so the withdrawal rate must be accurately set up to make sure that the optical thickness of each layer matches the $\lambda/4$ requirement. After a series of experiments, the appropriate withdrawal rates for individual layers were determined as 4200 μm/s and 3600 μm/s for the bottom and top layer, respectively.

Figure 4 shows the cross-sectional SEM image of a prepared double-layer ARC. The cross-section image shows a clear and identifiable boundary between the top and

bottom layers, and it could be seen that the film thickness of each layer was in good agreement with the design values.

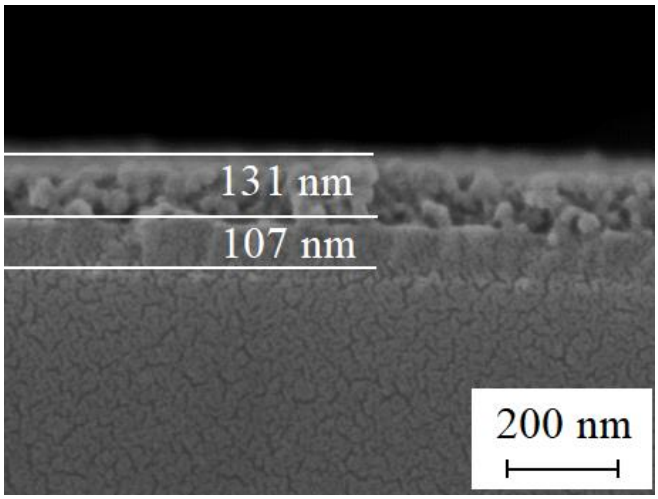

Figure 4. Cross-sectional SEM image of double-layer ARC.

Figure 5a shows the transmittance spectra of simulated and prepared double-layer broadband ARCs, and the transmittance spectrum of bare glass was also measured. Figure 5b shows the transmission spectra of experimental double-layer ARC in the region of 550–700 nm. Compared with bare glass, the transmittances of the prepared double-layer broadband ARC were significantly enhanced. The prepared double-layer ARCs can achieve consistent high transmittances with a fluctuation of 0.1% at 550–700 nm and the average transmittance at that region was 99.85%. At the region of 450–850 nm, the average transmittance was 99.25%. The transmittance spectrum of experimental double-layer ARCs was in good agreement with the transmittance spectrum of simulated double-layer ARCs (n_1 = 1.40 n_2 = 1.145) over most of the spectral range. The deviation was probably due to the light scattering, which was ignored at the simulated spectrum [27].

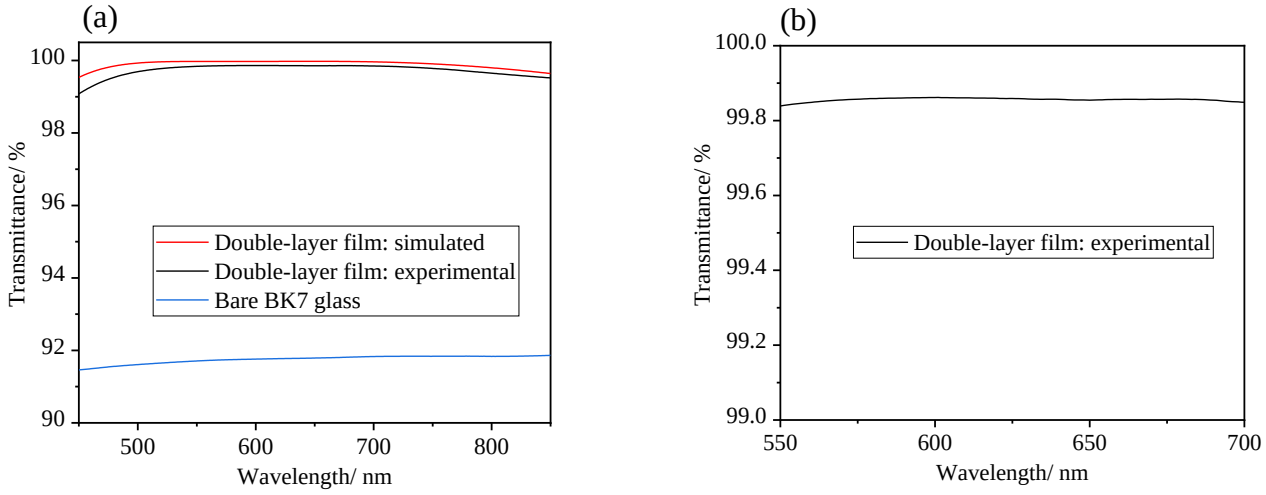

Figure 5. Transmission spectra of bare BK7 glass, simulated and experimental double-layer ARCs (**a**) and transmission spectra of experimental double-layer ARC in the region of 550–700 nm (**b**).

The light scattering is positively related to the roughness of the coatings. The roughness of the bottom layer, top layer, and double-layer coatings were analyzed by atomic force microscopy (AFM). As shown in Figure 6, the surface of the bottom layer coating (a) is relatively smooth compared to the top layer and double-layer coatings; the root-mean-square (R_q) is just 0.325 nm. The surfaces of the top layer (b) and double-layer coatings (c) are

both relatively rough; the root-mean-square (R_q) values are 5.57 and 4.65 nm, respectively. The root-mean-square (R_q) value of the double-layer coating stays at a low level, which is less than 5 nm, and the optical loss of experimental transmittance is less than 0.5% compared to that of simulated transmittance.

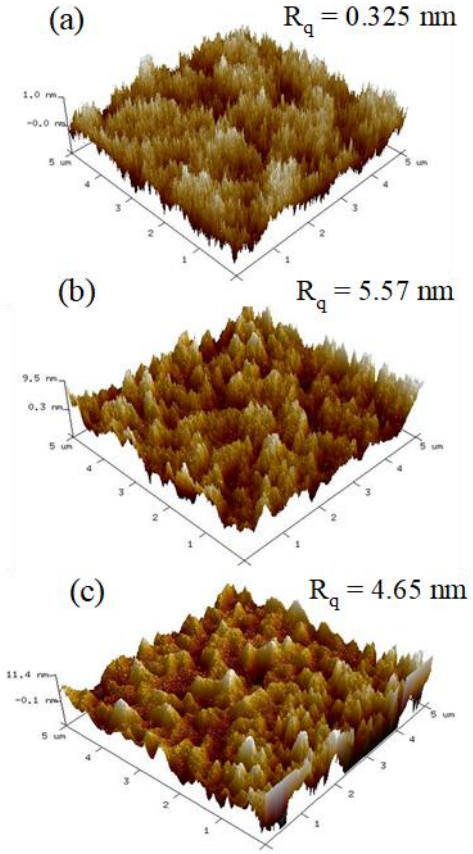

Figure 6. AFM 3D images of bottom layer coating (**a**), top layer coating (**b**) and double-layer coating (**c**).

3.4. Stability of Double-Layer ARC

In practical application, ARCs are often required to be resistant to humidity. In this study, to evaluate the stability of double-layer ARC in humid conditions, we measured the transmittance spectra of double-layer ARCs before and after being placed for two weeks at 25 °C and 50% relative humidity, and the result is shown in Figure 7.

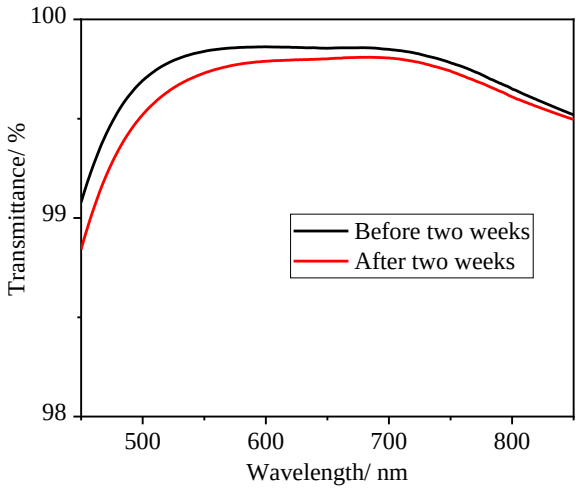

Figure 7. Transmittance spectra of double-layer ARC before and after two weeks.

Compared with regular base-catalyzed single-layer coatings with a 7–8% reduction in average transmittance after being placed for two weeks, the antireflective performance of the double-layer ARCs remained almost intact, and the reduction in average transmittance in the region of 450–850 nm was only 0.5%. The result shows that the double-layer ARC has good environmental stability.

4. Conclusions

Double-layer broadband ARCs with an average transmittance of 99.25% in the region of 450–850 nm were achieved using the sol–gel dip-coating process. The ARC with an outstanding optical property was prepared successfully and the transmittance achieved 99.7% with little fluctuation of 0.1% in the region of 550–700 nm. This double-layer ARC with good environmental stability has potential value in the fields of camera lenses, architectural glass, solar cells, high-power laser systems, and especially display panels.

Author Contributions: H.L., B.J. and J.L. conceived and designed the study, H.L. and P.W. performed the experiments and wrote the paper. Q.F. and P.X. provided technical support and reviewed the manuscript. All authors have read and agreed to the published version of the manuscript.

Funding: The funding support of the research is from the Petro China Scientific Research and Technology Development Project.

Institutional Review Board Statement: Not applicable.

Informed Consent Statement: Not applicable.

Data Availability Statement: Not applicable.

Conflicts of Interest: The authors declare no conflict of interest.

References

1. Chopra, K.L.; Paulson, P.D.; Dutta, V. Thin-film solar cells: An overview. *Prog. Photovolt.* **2004**, *12*, 69–92. [CrossRef]
2. Yao, L.; Qu, Z.; Pang, Z.L.; Li, J.; Tang, S.Y.; He, J.H.; Feng, L.L. Three-Layered Hollow Nanospheres Based Coatings with Ultrahigh-Performance of Energy-Saving, Antireflection, and Self-Cleaning for Smart Windows. *Small* **2018**, *14*, 1801661. [CrossRef]
3. Agustin-Saenz, C.; Machado, M.; Tercjak, A. Antireflective mesoporous silica coatings by optimization of water content in acid-catalyzed sol-gel method for application in glass covers of concentrated photovoltaic modules. *J. Colloid Interface Sci.* **2019**, *534*, 370–380. [CrossRef] [PubMed]
4. Cui, X.M.; Ding, R.M.; Wang, M.C.; Zhang, C.; Zhang, C.; Zhang, J.; Xu, Y. In Situ Surface Assembly Derived Ultralow Refractive Index MgF_2-SiO_2 Hybrid Film for Tri-Layer Broadband Antireflective Coating. *Adv. Opt. Mater.* **2016**, *4*, 722–730. [CrossRef]
5. Xing, Z.; Tay, S.W.; Ng, Y.H.; Hong, L. Porous SiO_2 Hollow Spheres as a Solar Reflective Pigment for Coatings. *ACS Appl. Mater. Interfaces* **2017**, *9*, 15103–15113. [CrossRef]
6. Wang, X.D.; Zhao, H.Y.; Cao, Y.Y.; Niu, Y.Y.; Shen, J. Sol-Gel Preparation of Laser Damage Resistant and Moisture-Proof Antireflective Coatings for KDP Crystals. *Langmuir* **2018**, *34*, 10262–10269. [CrossRef]
7. Zhao, H.Y.; Wang, X.D.; Feng, J.B.; Liu, Y.; Huang, J.C.; Shen, J. Environmental Stable SiO_2 Antireflective Coating Modified via NH3/HTMS Vapor Phase Treatment. *J. Inorg. Mater.* **2018**, *33*, 1219–1224. [CrossRef]
8. Zhang, Y.L.; Zhang, X.X.; Ye, H.P.; Yan, L.H.; Jiang, B. Design, Preparation and Modification of Third-Harmonic Silica Antireflective Coatings with Different Thickness. *Chin. J. Inorg. Chem.* **2012**, *28*, 119–124.
9. Zhang, S.; Xiao, P.; Wang, P.; Luo, J.; Jiang, B. Spherical-chain silica with super-hydrophobic surface and ultra-low refractive index for multi-functional broadband antireflective coatings. *Sol. Energy* **2020**, *207*, 1222–1230. [CrossRef]
10. Li, Y.-Y.; Jiang, B. lambda/4-lambda/2 Double-layer Broadband Antireflective Coatings with Superhydrophilicity and Photocatalysis. *J. Inorg. Mater.* **2019**, *34*, 159–163. [CrossRef]
11. Li, Y.Y.; Yang, K.; Xia, B.B.; Yang, B.W.; Yan, L.H.; He, M.Y.; Yan, H.W.; Jiang, B. Preparation of mechanically stable triple-layer interference broadband antireflective coatings with self-cleaning property by sol-gel technique. *RSC Adv.* **2017**, *7*, 14660–14668. [CrossRef]
12. Chuang, R.W.; Fu, K.L.; Zheng, Z.Y. The integrated vertically-coupled resistive random-access memory (ReRAM) based microdisk resonator and the relevant performance evaluation. In Proceedings of the Conference on Integrated Optics—Devices, Materials, and Technologies XXIV, Pl of SPIE OPTO Conference, San Francisco, CA, USA, 3–6 February 2020.
13. Mansano, R.D.; Ruas, R.; Mousinho, A.P.; Zambom, L.S.; Pinto, T.; Amoedo, L.H.; Massi, M. Use of diamond-like carbon with tungsten (W-DLC) films as biocompatible material. *Surf. Coat. Technol.* **2008**, *202*, 2813–2816. [CrossRef]
14. Zhu, B.Q.; Tao, H.Z.; Zhao, X.J. Effect of buffer layer on thermochromic performances of VO2 films fabricated by magnetron sputtering. *Infrared Phys. Technol.* **2016**, *75*, 22–25. [CrossRef]

15. Fahland, M.; Kirchhoff, V.; Schiller, N.; Schiller, S. High rate deposition of oxide layers by pulsed magnetron sputtering (PMS) for display manufacturing. *ITG-Fachber* **1998**, *150*, 179–183.
16. Lee, J.H.; Eun, J.H.; Park, S.Y.; Kim, S.G.; Kim, H.J. Hydration of r.f. magnetron sputtered MgO thin films for a protective layer in AC plasma display panel. *Thin Solid Film.* **2003**, *435*, 95–101. [CrossRef]
17. Kim, J.Y.; Kim, E.R.; Han, Y.K.; Nam, K.H.; Ihm, D.W. Highly transparent tin oxide films prepared by DC magnetron sputtering and its liquid crystal display application. *Jpn. J. Appl. Phys. Part 1 Regul. Pap. Short Notes Rev. Pap.* **2002**, *41*, 237–240. [CrossRef]
18. Helmersson, U.; Lattemann, M.; Bohlmark, J.; Ehiasarian, A.P.; Gudmundsson, J.T. Ionized physical vapor deposition (IPVD): A review of technology and applications. *Thin Solid Film.* **2006**, *513*, 1–24. [CrossRef]
19. Choy, K.L. Chemical vapour deposition of coatings. *Prog. Mater. Sci.* **2003**, *48*, 57–170. [CrossRef]
20. Li, Y.; Lv, H.; Ye, L.; Yan, L.; Zhang, Y.; Xia, B.; Yan, H.; Jiang, B. Preparation of porous silica films in a binary template system for double-layer broadband antireflective coatings. *RSC Adv.* **2015**, *5*, 20365–20370. [CrossRef]
21. Tang, X.N.; Yan, X. Dip-coating for fibrous materials: Mechanism, methods and applications. *J. Sol-Gel Sci. Technol.* **2017**, *81*, 378–404. [CrossRef]
22. Zhang, S.; Zhao, X.; Wang, P.; Xiao, P.; Luo, J.; Jiang, B. Preparation of superhydrophilic silicate coating by sol-gel for double-wavelength broadband antireflective coatings. *J. Sol-Gel Sci. Technol.* **2019**, *92*, 598–606. [CrossRef]
23. Meakin, P.; Jullien, R. The effects of restructuring on the geometry of clusters formed by diffusion-limited, ballistic, and reaction-limited cluster cluster aggregation. *J. Chem. Phys.* **1988**, *89*, 246–250. [CrossRef]
24. Yang, J.; Chen, J.R.; Yu, R. Surface wettability and vapour stability of silica membranes modified by sol-gel method. *J. Inorg. Mater.* **2008**, *23*, 739–744. [CrossRef]
25. Qu, L.; Rahimi, S.; Qian, J.; He, L.; He, Z.; Yi, S. Preparation and characterization of hydrophobic coatings on wood surfaces by a sol-gel method and post-aging heat treatment. *Polym. Degrad. Stab.* **2021**, *183*, 109429. [CrossRef]
26. Vidal, K.; Gomez, E.; Martinez Goitandia, A.; Angulo-Ibanez, A.; Aranzabe, E. The Synthesis of a Superhydrophobic and Thermal Stable Silica Coating via Sol-Gel Process. *Coatings* **2019**, *9*, 627. [CrossRef]
27. Nayar, S.K.; Ikeuchi, K.; Kanade, T. Surface reflection—Physical and geometrical perspectives. *IEEE Trans. Pattern Anal. Mach. Intell.* **1991**, *13*, 611–634. [CrossRef]